Published in final edited form as:
Bone. 2014 May ; 62: 1–9. doi:10.1016/j.bone.2014.01.021.

The Loss of Activating Transcription Factor 4 (ATF4) Reduces Bone Toughness and Fracture Toughness

Alexander J. Makowski[1,2], **Sasidhar Uppuganti**[3], **Sandra A. Waader**[1], **Jack M. Whitehead**[3], **Barbara J. Rowland**[1,4], **Mathilde Granke**[3], **Anita Mahadevan-Jansen**[2], **Xiangli Yang**[4,5], and **Jeffry S. Nyman**[1,2,3,4]

[1]Department of Veterans Affairs, Tennessee Valley Healthcare System, Nashville, TN 27212

[2]Department of Biomedical Engineering, Vanderbilt University, Nashville, TN 37232

[3]Department of Orthopaedic Surgery & Rehabilitation, Vanderbilt University Medical Center, Nashville, TN 37232

[4]Center for Bone Biology, Vanderbilt University Medical Center, Nashville, TN 37232

[5]Department of Medicine, Vanderbilt University Medical Center, Nashville, TN 37232

[6]Department of Pharmacology, Vanderbilt University Medical Center, Nashville, TN 37232

Abstract

Even though age-related changes to bone tissue affecting fracture risk are well characterized, only a few matrix-related factors have been identified as important to maintaining fracture resistance. As a gene critical to osteoblast differentiation, activating transcription factor 4 (ATF4) is possibly one of the seimportant factors. To test the hypothesis that the loss of ATF4 affects the fracture resistance of bone beyond bone mass and structure, we harvested bones from *Atf4*+/+ and *Atf4*−/− littermates at 8 and 20 weeks of age (n≥9 per group) for bone assessment across several length scales. From whole bone mechanical tests in bending, femurs from *Atf4*−/− mice were found to be brittle with reduced toughness and fracture toughness compared to femurs from *Atf4*+/+ mice. However, there were no differences in material strength and in tissue hardness, as determined by nanoindentation, between the genotypes, irrespective age. Tissue mineral density of the cortex at the point of loading as determined by micro-computed tomography was also not significantly different. However, by analyzing local composition by Raman Spectroscopy (RS), bone tissue of *Atf4*−/− mice was found to have higher mineral to collagen ratio compared to wild-type tissue, primarily at 20 weeks of age. From RS analysis of intact femurs at 2 orthogonal orientations relative to the polarization axis of the laser, we also found that the organizational-sensitive peak ratio, ν1 Phosphate per Amide I, changed to a greater extent upon bone rotation for Atf4-deficient tissue, implying bone matrix organization may contribute to the brittleness phenotype. Target

Correspondence: Jeffry S. Nyman, Vanderbilt Orthopaedic Institute, Medical Center East, South Tower, Suite 4200, Nashville, TN 37232, jeffry.s.nyman@vanderbilt.edu o: (615) 936-6296 f: (615) 936-0117.

genes of ATF4 activity are not only important to osteoblast differentiation but also maintaining bone toughness and fracture toughness.

Keywords

Bone Quality; Fracture Toughness; Micro-Computed Tomography; Raman; Collagen

Introduction

The age-related increase in fracture risk is not solely due to a loss in bone mineral density [1], and by extension a decline in bone strength, leading to the idea that the inherent quality of bone tissue is an important attribute of fracture resistance. With respect to the apparent material properties of bone, there is a greater loss in cortical bone toughness with aging than in bone strength [2](−8.7% per decade vs. −4.7% per decade [3]). In addition to the age-related decrease in post-yield energy dissipation [4], the capacity of human cortical bone to resist crack growth (fracture toughness) diminishes with advancing age as determined by strain energy release rate (G_c), critical stress intensity factor (K_c), J-integral, and R-curve behavior (crack propagation toughness) [5–9]. Despite the critical role of collagen as a determinant of bone toughness (i.e., lack of brittleness)[10–12] and fracture toughness [13–15], there is an incomplete understanding of what exactly regulates these material properties of bone.

Recent analyses of long bones from different genetic mouse models have started to identify genes that may be important in promoting the ability of the bone tissue to resist fracture, beyond influencing bone strength. For example, deletion of the proteolysis genes, matrix metalloproteinase (MMP)-9 and MMP-13 separately, produced a brittle bone phenotype (e.g., low post-yield deflection) [16,17]. Deletion of non-collagenousproteins, namelyosteopontin (OPN) and osteocalcin (OCN) separately or concurrently, resulted in bones with lower fracture toughness in relation to long bones from wild-type mice [18,19]. Acquiring femurs from genetic and transgenic mice in which transforming growth factor-beta (TGF-β) signaling was either low, normal or high, Balooch et al. [20] provided the first link between a growth factor and fracture toughness: resistance to crack growth was inversely proportional to TGF-β signaling.

The activating transcription factor 4 (ATF4) is another possible gene important to promoting the toughness and fracture toughness of bone. Transcription factors determine cell fate, and in the case of osteoblasts, ATF4 activity promotes the expression of the aforementioned OCN [21]. Moreover, osteoblasts lacking ATF4 do not fully mature and do not adequately synthesize type 1 collagen as amino acid transport is diminished in ATF-deficient osteoblasts (in vitro) [21]. Thus, *Atf4*−/− mice have smaller bones and less trabecular bone volume fraction than *Atf4*+/+ mice. To date, there is scant evidence that transcription factors regulate the fracture resistance of bone from the perspective of energy dissipation during fracture. Understandably, toughening mechanisms are multifactorial given the hierarchical organization of bone's constituents. Nonetheless, evidence that the loss of a transcription factor affects bone toughness or fracture toughness opens avenues of research into novel

therapeutic targets that go beyond stimulating more bone (or preventing loss of bone) to generating better bone tissue with high resistance to fracture. Toward this end, we hypothesized that the loss of ATF4 lowers bone's resistance to fracture through changes in the matrix, not necessarily due to deficits in bone structure and mineral density.

Materials and Methods

Tissue Collection

Mice lacking 1 copy of ATF4 were re-derived onto a FVB background from an existing colony [21] (C57BL/6 background) because bones from the C57BL/6 strain have relatively low ash fraction [22,23] and do not readily snap during load-to-failure tests in the three point bending configuration when acquired from young mice. Breeding *Atf4*+/− mice generated *Atf4*+/+ (n≥12 per age group) and *Atf4*−/− littermates (n=9 per age group) that were euthanized at 8 and 20 weeks of age following a protocol approved by the local IACUC. Femurs and the L6 vertebrae were frozen in phosphate buffered saline (PBS) for biomechanical testing, while tibiae were dehydrated in ethanol and embedded in polymethylmethacrylate (PMMA) [24]. For Raman Spectroscopy (RS) and nanoindentation, transverse cross sections were cut at the mid-shaft (~6 mm thick in a region above the tibia-fibula junction) using a diamond embedded band saw (310, EXAKT Technologies, Inc., Oklahoma City, OK). The proximal surface of the embedded section was ground on successive grits of silicon carbide paper using a precision grinder (400CS, EXAKT Technologies, Inc., Oklahoma City, OK) and then polished on synthetic cloth (Master Tex, Buehler, Lake Bluff, IL)with alumina solution(Master Prep 0.05 μm, Buehler, Lake Bluff, IL), [16] using a polisher (VibroMet 2, Buehler, Lake Bluff, IL). The posterior side of the right femur from each mouse was micro-notched for fracture toughness testing using first a low speed, diamond-embedded saw, and then a razorblade coated with a diamond solution [18].

Micro-Computed Tomography Analysis

Prior to mechanical testing, the mid-shafts of the un-notched, left femurs and the L6 VBs were scanned (μCT40, Scan co Medical, Brüttisellen, Switzerland)at an isotropic voxel size of 12 μm using the same settings (70 kVp/114 μA; 1000 projections per 360° rotation; and 300 ms integration time) and a hydroxyapatite (HA) phantom calibration with the manufacturer's beam hardening correction. To calculate structural properties (Ct.Th, Ct.Ar, I_{min}, etc.) and tissue mineral density of cortical bone (Ct. TMD), contours were fit to the outer cortex. To calculate the architectural properties (BV/TV, Tb.N, Conn.D, etc.) and TMD of trabecular bone (Tb.TMD), contours were drawn by hand inside the cortical shell of the VB for each slice between the endplates. The segmentation procedure was consistent among all scans per bone type: global thresholds (and a Gaussian filter to suppress image noise) of 715.2 mgHA/cm^3 (sigma=0.8 with support of 2) for cortical and 421.3 mgHA/cm^3 (sigma=0.3 with support of 1) for trabecular bone. The central mid-shaft of the notched, right femurs were scanned at an isotropic voxel size of 6 μm using the same scanner and scan conditions. Contours were fit to the outer cortex above and below the notched region to determine the mean centroid, cortical thickness (Ct.Th), mean radius of the cortex ((c_{min} +

c_{max})/2), and Ct.TMD. The notched region was evaluated to ensure proper size and to determine the angle of the notch (2θ).

Whole-Bone Biomechanical Testing

Three point bending tests of hydrated, un-notched [16] and notched femurs [5] were conducted using a bench-top, material testing system (Dynamight 8841, Instron, Canton, OH). For the un-notched bones, the span (L) and loading rate were 8 mm and 3 mm/min, respectively. For the notched femurs, the span was 4 times the mean outer anterior-posterior diameter (i.e., in the direction of loading) of each group. The loading rate of these femurs was 0.06 mm/min. Force vs. displacement data were recorded at 50 Hz from a 100 N load cell (Honeywell,, OH) and the linear variable displacement transducer.

In mechanical analysis of the un-notched femur, whole bone stiffness was the slope of the initial linear portion of the curve and strength was the peak force (P_f) endured by the mid-shaft. Using the moment of inertia (I_{min}) of the mid-shaft and the distance between the centroid and the bone surface in the anterior-posterior direction (c_{min}) from μCT, we estimated the modulus and strength from standard flexural equations [25]. The yield point was deemed to occur when the secant stiffness was 15% less than the initial stiffness. Post-yield deflection (PYD) was then defined as the displacement at fracture minus displacement at yielding, and post-yield toughness was defined as the area under the force vs. displacement curve after yielding divided by the bone cross-sectional area (Ct.Ar) [26]. K_c was quantified assuming the stress intensity at the micro-notch root is similar to that of a circumferential through-wall crack in a thin-wall cylinder subjected to bending [27]:

$$K_c = F_b \frac{P_f L R_o}{\pi (R_o^4 - R_i^4)} \sqrt{\pi R_m \theta_c} \quad \text{eq. (1)}$$

where the outer, inner, mean radius (R_o, R_i, and R_m) of the bone cortex, and the half-crack angle (θ) were determine using μCT. Confirming the ratio *Rm/Ct.Th* was less than 80.5 and greater than 1.5 and that θ_{init} was less than 110° and greater than 0, the geometry factor (F_b) was calculated using the equation published by Takahashi [28]. In addition, scanning electron microscopy (SEM) imaging of the fracture surface after fracture toughness testing was used to determine the θ at which crack propagation transitioned from stable to instable (θ_{inst}). The instability K ($K_{c,\,inst}$) was calculated using the final force at fracture for θ_{inst} (eq. 1).

Each hydrated VB was subjected to axial compression at 3 mm/min in which the supporting platen had a rough surface and a moment relief to minimize slippage and off-axis loading, respectively. Moreover, all tests were recorded with a high-resolution camera (Canon E6, Canon, Melville, NY) with a macro lens. We observed that 2 VBs were not tested properly as they moved laterally during compression. Data from these two bones were not included in the analysis.

Tissue-level Assessment

Prior to nanoindentation, 9 spectra (spaced around the cross section) were acquired from each embedded bone using a standard confocal Raman microscope (RenishawInVia Raman

Microscope, Renishaw, Hoffman Estates, IL) equipped with a 50× (NA=0.75) objective, a 35 μm slit opening, and a 785 nm laser diode source (Innovative Photonic Solutions, Monmouth Junction, NJ). Each spectrum consisted of 5 accumulations of 30s integration time to yield a high signal to noise ratio (SNR) from 300 to 1800 cm^{-1} (Hydroxyproline SNR in excess of 25:1). Spectra were processed via least squares modified polynomial fit [29] and smoothed for noise using an 2^{nd} order Savitsky-Golay filter [30]. Custom Matlab software (Mathworks, Natick, MA) extracted the intensity and wave number of the prominent spectral. There was no spectral binning in this analysis.

Twelve indents (4 per side) were attempted throughout the tibia cross-section using a nanoindenter (XP, MTS, Eden Prairie, MN) equipped with a Berkovich diamond tip. Loading at a constant strain rate to a depth of 1 μm and then unloading after a 30 s dwell, nanoindentation modulus and hardness of the tissue (0.25 μm resolution) were calculated from the slope of the upper unloading portion of the force vs. displacement curve and the peak force, respectively, as described by Oliver and Pharr [31]. Data was excluded if either the force displacement curve or post-hoc optical examination of the indent site revealed the presence of sub-surface pores.

Prior to fracture toughness testing, the anterior side of the right femoral mid-shaft was placed under the 50× objective of the Raman InVia microscope. Using mid-shaft vessel perforations as landmarks to consistently select the site of analysis across bones, spectra were collected at two intact bone orientations: 0° and 90° relative to the polarization axis of the incident laser, which had an approximate extinction ratio of 1:200 (i.e., light was not fully polarized by adding optics). Laser power and exposure time were optimized to achieve SNR similar to embedded samples. Co-localization of spectral collection sites was accomplished manually by registering fine structural features in the bright field.

To determine differences in composition among the experimental groups, we averaged the Raman measurements per bone. The Raman properties of interest included:ν1 Phosphate (961 − 962 cm^{-1}) per Amide I (1667– 1670 cm^{-1}), ν1 Phosphate per Proline (855 – 858 cm^{-1}), ν2 Phosphate (430 – 431 cm^{-1}) per Amide III (1248 – 1252 cm^{-1}), Carbonate (1072 – 1073 cm^{-1}) per ν1 Phosphate, and the inverse of the full-width at half maximum of ν1 Phosphate peak ($[FWHM]^{-1}$). Because ν1 Phos/Am I is sensitive to polarization bias (i.e., collagen fibril orientation) while ν1 Phos/Proline and ν2 Phos/Am III are less so [24,32], we examined how a change in bone orientation shifted the regression lines among the mineral to collagen ratios (MCR) for each genotype as a way to infer differences in matrix organization.

Statistical analysis

A two-way analysis of variance (ANOVA) determined whether age and genotype affected each property. Pair-wise comparisons were then tested for significance using either Student's t-test (parametric) or Mann-Whitney (non-parametric) depending on normality and homoscedasticity of each data set. Differences were deemed significant at a p-value adjusted by the Šidák correction for multiple hypothesis testing. Analysis of Covariance determined whether linear relationships (i.e., intercept and slope) between peak force and moment of inertia were different between genotypes. To examine the effect of bone rotation on the

MCR relationships, the data were pooled across age groups within genotype and then bootstrapped in order to fit general linear models with the initial independent variables being peak ratio, orientation, and their interaction. Equations were recorded for models with the highest possible R^2 value. Statistical analysis was performed using Stata (v11, StataCorp, College Station, TX).

Results

ATF4 deletion affected trabecular bone architecture and cortical bone structure

Verifying that the rederivation of the *Atf4*+/− mice on a different background strain did not affect the published phenotype, trabecular bone volume fraction of the L6 VB was much lower for the *Atf4*−/− than for the *Atf4*+/+ mice, irrespective of age (Table 1). There were also architectural differences between the genotypes with Atf4-deficient VBs having fewer trabeculae, thinner trabeculae, and lower connectivity density (Table 1). Tissue mineral density of the trabecular bone however was not different between the genotypes. Still, the low BV/TV was sufficient enough that *Atf4*−/− VBs were weaker in compression than the *Atf4*+/+ VBs.

Loss of ATF4 affected cortical bone structure as well in that the null femur shad a thinner cortex, smaller medullary volume, and a lower moment of inertia, regardless of age (Table 2). As with the trabecular bone, Ct.TMD increased with age for each genotype, but the difference between genotypes was not strictly significant (Table 2). Nonetheless, matching the trends in bone structure, the femurs from the knock-out mice were less stiff and weaker in bending than those from wild-type mice. Moreover, at 20 wk of age, the ability of the *Atf4*−/− bone to deform after yielding was nearly half that of the *Atf4*+/+ bone (Table 2).

Loss of ATF4 decreased bone toughness with no effect on material strength

Upon factoring out the structural contribution to whole bone strength as determined by peak force, we found that the estimated material strength of the mid-shaft was not different between *Atf4*+/+ and *Atf4*−/− mice (Fig. 1). This observation concurs with the lack of a demonstrable difference in Ct.TMD between the genotypes. To further confirm that the difference in whole bone strength was primarily due to a structural difference between the genotypes, not differences in tissue properties, we compared the slopes and y-intercepts of the regression lines for each genotype's peak force versus moment of inertia relationship. As shown for 20 wk bones, there were no differences in the regression parameters (Fig 1). The *Atf4*−/− femurs were clearly more brittle with substantially lower post-yield work-to-fracture per bone cross-sectional area (Fig 1). The difference in post-yield toughness was more pronounced at 20 wks of age than at 8 wks of age. As further confirmation of fracture resistance phenotype unrelated to material strength, the fracture toughness was lower for the 20 wk old *Atf4*−/− mice than for the 20 wk old *Atf4*+/+ mice (Fig. 2).

ATF4 deletion had differential effects on tissue-level properties between age groups

Nanoindentation of the embedded bone tissue did not reveal differences in modulus and hardness between the genotypes, although there was a trend of a lower modulus for the ATF4-deficient tissue at 8 wk (Table 3). The significant age-related increase in these

properties for both genotypes was likely related to the age-related increase in mineralization (Table 2). Interestingly, the MCR, as determined by the polarization (organization)-sensitive ν1Phos/AmI was less in the *Atf4*−/− tibia than in the *Atf4*+/+ tibia (Table 3). This peak ratio increased more with age for the knock-out mice than for the wild-type mice. As such, the genotype difference at 20 wk of age trended toward ν1Phos/AmI being higher, not lower, in the ATF4-deficient tissue. The polarization-insensitive ν2Phos/AmIII acquired from the tibia cross-section was not different at 8 wk between genotypes but was greater in the ATF4-deficient tissue suggesting a compositional difference in the mineral relative to the collagen existed between *Atf4*−/− and *Atf4*+/+ mice with skeletal maturity (Table 3). Other differential effects of ATF4-deficiency between age groups include higher type B carbonate substitution (Carb/ν1Phos) and lower crystallinity ($[FWHM]^{-1}$) with the loss of ATF4 in only the 8 wk group (no differences in the 20 wk group; Table 3).

ATF4 deletion possibly affected matrix organization in addition to composition

To identify the potential origins of the brittle bone phenotype of the *Atf4*−/− mice, we compared the effect of ATF4-deficiency on the volumetric TMD of the mid-shaft cortex (by μCT) to its effect on MCR (by RS), acquired from the same intact femur mid-shaft (i.e., the notched femurs prior to testing). As was observed for the un-notched bone, Ct.TMD was greater for femurs from 20 wk than from 8 wk mice with little difference between genotypes at each age (Fig. 3A). In contrast, the Raman-derived MCR measurements (ν1Phos/Proline, ν2Phos/AmIII, and ν1Phos/AmI) from the outer cortex of the mid-shaft (anterior side) did not increase with age in the *Atf4*+/+ bone and had a modest increase with age in the *Atf4*−/− bone (Fig. 3B). This suggests that the amount of mineral relative to collagen in the cortex did not vary between 8 wk and 20 wk of age in wild-type mice. In contrast, there was more mineral relative to collagen (or less collagen relative to mineral) with the loss of ATF4 by 20 wk(Fig. 3B).

To gain further insight into whether differences in tissue organization existed between the genotypes, we examined the effect of rotating the intact femur on the relationships among the three peak ratios representing MCR (Fig. 4). As expected, the regression line for the longitudinal orientation overlapped that of the orthogonal orientation when plotting ν2Phos/AmIII versus ν1Phos/Proline, irrespective of genotype (Fig. 4A & 4B) because these peak ratios are relatively insensitive to polarization bias [32,33]. When plotting each insensitive peak ratio versus the polarization-sensitive ν1Phos/AmI (Fig. 4C & 4E), there was a shift in the regression line for the wild-type bone such that the y-intercept, but not the slope, depends on orientation of the bone relative to the polarization angle of the incident light (Table 4). Interestingly, the slope of these regression lines changes upon bone rotation from the longitudinal to the orthogonal orientation (Fig. 4D & 4F) for only the *Atf4*−/− bone (Table 4). The differential effect of bone orientation on MCR regressions between genotypes suggests an underlying tissue organizational phenotype exists with loss of ATF4.

Discussion

Strength is not the only property that characterizes the ability of bone to resist fracture. Fracture risk can increase because bone loses the ability i) to sustain deformation after the

on-set of permanent deformation (i.e., yield point), ii) to minimize microdamage accumulation, or iii) to resist crack growth. As with other materials subjected to dynamic loads, fracture resistance of bone depends on several properties such asi) toughness, ii) fatigue endurance, and iii) fracture toughness, respectively. Although aging and certain diseases affect these characteristics(e.g., rheumatoid arthritis [34], duration of high fat diet [35,36], and osteogenesis imperfect [37]), there is little known about critical regulators of the bone matrix that promote toughening mechanisms. Presently, we provide evidence that a transcription factor important to osteoblast differentiation influences both the toughness and the fracture toughness of bone (at the material level) in addition to proper cortical bone structure and trabecular bone architecture (at the whole bone level).

The reduction in bone toughness and fracture toughness in the *Atf4*−/− mice compared to the *Atf4*+/+ mice could be due to an imbalance of mineral accumulation relative to the organic matrix. As determined by μCT in mgHA/cm^3, there was little difference in the TMD between the genotypes (Table 1, Table 2, and Fig. 3) with TMD increasing with skeletal maturation or age in both genotypes. However, as determined by Raman spectroscopy on embedded tibia cross-sections and intact femurs, the relative amount of mineral to the amount of collagen did not vary between 8 weeks and 20 weeks of age in wild-type mice but did so in knock-out mice (Table 3 and Fig. 3B, 3C, & 3D). Taken together, these observations suggest that normal mineral accumulation outpaced reduced collagen deposition [21] in the ATF4-deficient bones with respect to wild-type bones. Of note, bone formation rate is lower with the loss of ATF4 [21] suggesting tissue age, a determinant of the degree of mineralization, varied between the genotypes. In general, mineral density and collagen are the primary determinants of material strength and toughness, respectively [38], but bones with higher degree of mineralization (or ash fraction) have lower toughness than bones with lower mineralization [39]. Thus, matching the trends in tissue composition (no difference in TMD but greater MCR with ATF4 deficiency), there was not a significant difference in peak bending strength between the genotypes (Fig. 1), but the post-yield deflection (Table 2) and fracture toughness (Fig. 2) were lower for bones from the 20 wk*Atf4*−/− mice.

The deletion of ATF4 also appeared to affect tissue organization. Although we do not have direct measurements of fibril orientation, we can infer organization-related differences by examining the effect of bone rotation on there gressions among the RS-derived MCRs. This is possible because bone tissue is a birefringent material, and ν1Phos/AmI is sensitive to polarization when the RS instrument does not depolarize the laser light (diode lasers are inherently polarized even without added optics)[33]. That is, for the same location with a given MCR and collagen fibril orientation, ν1Phos/AmIdepends on the predominant angle of the polarized light relative to the predominant direction of the collagen fibrils. If the collagen fibrils at the site of measurement are randomly orientated (i.e., isotropic), then ν1Phos/AmI would have minimal change upon rotation. However, mineralized collagen fibrils of bone typically have preferentially orientation that can shift from region to region [40,41]. Thus, there is a shift in the regression line forν1Phos/AmIversusν1Phos/Proline, a polarization-insensitive peak ratio, going from longitudinal to orthogonal bone orientation (Figure 4). Interestingly, the shift is greater for the ATF4-deficient bone (see horizontal lines

in Figure 4). This could be due to an overall difference in fibril direction or a difference in the net distribution of the collagen fibrils (anisotropy) between the genotypes. With respect to the latter possibility, the greater shift suggests the tissue anisotropy was greater or organizational heterogeneity was less for ATF4-deficient bone. This remains to be confirmed.

Identifying the origins of bone brittleness is challenging because toughening mechanism exist at multiple length scales. Thus, there could be other explanations for why bones from *Atf4*−/− have lower toughness and fracture toughness than bones from control littermates. Surveying reports of other bone brittleness phenotypes, cortical bone from osteopontin (OPN)-deficient mice has local regions of hyper-mineralization and more anisotropic collagen fibrils compared to the tougher bones from *Opn*+/+ mice [18]. Similarly, in comparison to wild-type mice with higher bone toughness and fracture toughness, the cortical bone from *Mmp*13−/− mice has local regions of hyper-mineralized tissue as well as increases in non-enzymatic collagen cross links and disrupted birefringent lamellar bands [17]. Thus, a common theme in genetic models with a bone brittleness phenotype is a disruption in normal mineralization and collagen organization. As is the case with these previous studies in which the gene was deleted in all cells, we cannot definitively conclude that the regulation of matrix properties by ATF4 is solely osteoblast-specific.

Given that a major downstream target of ATF4 is *Ocn* gene [21,42][43,44], the biomechanical phenotype of OCN-deficient mice could be similar to that of ATF4-deficient mice. With respect to toughness, there is similarity in that the bone from *Ocn*−/− mice have a lower propagation toughness than bone from wild-type mice [19]. Being a charged molecule with Ca^{2+} binding sites, OCN may directly promote resistance to cracking [19] by acting as a sacrificial bond between mineralized collagen fibrils [45,46]. While there are similarities in the brittleness phenotype of the *Atf4*−/− and *Ocn*−/− mice, OCN-deficiency does not lower the structural strength of whole bones in intact mice [47]. This is different than what we observe for the bone of *Atf4*−/− mice (Table 2). In addition, unlike the effect of ATF4 deficiency on MCR, there was no difference in the mineral to matrix ratio [48] as determined by Fourier transformed infrared spectroscopy or in ν1Phos/AmI as determined by RS [49] between adult (6 mo. and 12 mo.) *Ocn*−/− and *Ocn*+/+ mice. Thus, while ATF4 activity may certainly regulate bone brittleness through OCN, other protein sunder ATF4 control are likely influencing the fracture resistance of bone.

With respect to its role in bone, ATF4 was initially discovered to be the other transcription factor, along with Runx2, that binds the promoter region of the osteocalcin gene [21]. ATF4 is a downstream target of two important factors in bone maintenance: transforming growth factor beta (TGF-β) and intermittent parathyroid hormone (PTH) [44,50]. Among other actions in bone, TGF-β signaling preserves the osteoprogenitor pool at the expense of differentiation [51], and we previously found that suppressing TGF-β with a neutralizing antibody increased trabecular bone volume in *Atf4*+/+ mice but not in *Atf4*−/− mice [50]. Similarly in an earlier study, Yu et al. [52] found that the anabolic effect of intermittent recombinant parathyroid hormone (hPTH(1–34)) on bone was abrogated in growing *Atf4*−/− mice as well as mature, ovariectomized*Atf4*−/− mice relative to PTH-treated littermate controls. As further evidence of the interest in ATF4 as a critical mediator of bone

maintenance, high expression of a micro RNA (miR-214) was recently found to be associated with fractures, and miR-214 was shown to down-regulate ATF4, thereby inhibiting osteoblast activity [53]. The findings of the present study suggest that suppressing ATF4 does more than reduce bone formation: suppression or specifically the loss of ATF4 can lead to bone brittleness.

Conclusions

The loss of ATF4 results in a brittle bone phenotype that becomes more severe with skeletal maturity and includes a loss in fracture toughness but no decrease in material strength. Accompanying the difference in bone toughness between *Atf4*−/− and *Atf4*+/+ mice is a higher mineral to collagen ratio and more fibril anisotropy with ATF4 deficiency. The lack of a difference in material strength (independent of structure) between the genotypes concur with the lack of significant difference in tissue mineral density, making the ATF4-null model a strong candidate for examination of the underlying mechanisms of toughness, as well as for the evaluation of therapeutics that target bone toughness and resistance to crack propagation.

Acknowledgments

This material is based upon work supported by the Department of Veterans Affairs, Veterans Health Administration, Office of Research and Development. We thank George M. Pharr and Erick G. Herbert for access to their nanoindenter.

REFERENCES

1. Kanis JA, Johnell O, Oden A, Dawson A, De Laet C, Jonsson B. Ten year probabilities of osteoporotic fractures according to BMD and diagnostic thresholds. Osteoporos Int. 2001; 12:989–995. [PubMed: 11846333]
2. Burstein AH, Reilly DT, Martens M. Aging of bone tissue: mechanical properties. J Bone Joint Surg Am. 1976; 58:82–86. [PubMed: 1249116]
3. Zioupos P, Currey JD, Hamer AJ. The role of collagen in the declining mechanical properties of aging human cortical bone. J Bio med Mater Res. 1999; 45:108–116.
4. Nyman JS, Roy A, Tyler JH, Acuna RL, Gayle HJ, Wang X. Age-related factors affecting the post yield energy dissipation of human cortical bone. J Orthop Res. 2007; 25:646–655. [PubMed: 17266142]
5. Yeni YN, Brown CU, Norman TL. Influence of bone composition and apparent density on fracture toughness of the human femur and tibia. Bone. 1998; 22:79–84. [PubMed: 9437517]
6. Zioupos P, Currey JD. Changes in the stiffness, strength, and toughness of human cortical bone with age. Bone. 1998; 22:57–66. [PubMed: 9437514]
7. Zioupos P. Accumulation of in-vivo fatigue micro damage and its relation to biomechanical properties in ageing human cortical bone. J Microsc. 2001; 201:270–278.
8. Nalla RK, Kruzic JJ, Kinney JH, Ritchie RO. Effect of aging on the toughness of human cortical bone: evaluation by R-curves. Bone. 2004; 35:1240–1246. [PubMed: 15589205]
9. Zimmermann EA, Schaible E, Bale H, Barth HD, Tang SY, Reichert P, et al. Age-related changes in the plasticity and toughness of human cortical bone at multiple length scales. Proceedings of the National Academy of Sciences. 2011; 108:14416–14421.
10. Currey JD, Foreman J, Laketić I, Mitchell J, Pegg DE, Reilly GC. Effects of ionizing radiation on the mechanical properties of human bone. J Orthop Res. 1997; 15:111–117. [PubMed: 9066534]
11. Wang X, Bank RA, TeKoppele JM, Agrawal CM. The role of collagen in determining bone mechanical properties. J Orthop Res. 2001; 19:1021–1026. [PubMed: 11781000]

12. Unger S, Stefan U, Blauth M, Michael B, Schmoelz W, Werner S. Effects of three different preservation methods on the mechanical properties of human and bovine cortical bone. Bone. 2010; 47:1048–1053. [PubMed: 20736094]
13. Mitchell EJ, Stawarz AM, Kayacan R, Rimnac CM. The effect of gamma radiation sterilization on the fatigue crack propagation resistance of human cortical bone. J Bone Joint Surg Am. 2004; 86-A:2648–2657. [PubMed: 15590849]
14. Yan J, Daga A, Kumar R, Mecholsky JJ. Fracture toughness and work of fracture of hydrated, dehydrated, and ashed bovine bone. Journal of Biomechanics. 2008; 41:1929–1936. [PubMed: 18502430]
15. Barth HD, Zimmermann EA, Schaible E, Tang SY, Alliston T, Ritchie RO. Characterization of the effects of x-ray irradiation on the hierarchical structure and mechanical properties of human cortical bone. Biomaterials. 2011; 32:8892–8904. [PubMed: 21885114]
16. Nyman JS, Lynch CC, Perrien DS, Thiolloy S, O'quinn EC, Patil CA, et al. Differential effects between the loss of MMP-2 and MMP-9 on structural and tissue-level properties of bone. J Bone Miner Res. 2011; 26:1252–1260. [PubMed: 21611966]
17. Tang S, Herber R-P, Ho S, Alliston T. Matrix metalloproteinase-13 is required for osteocytic perilacunar remodeling and maintains bone fracture resistance. J Bone Miner Res. 2012
18. Thurner PJ, Chen CG, Ionova-Martin S, Sun L, Harman A, Porter A, et al. Osteopontin deficiency increases bone fragility but preserves bone mass. Bone. 2010; 46:1564–1573. [PubMed: 20171304]
19. Poundarik AA, Diab T, Sroga GE, Ural A, Boskey AL, Gundberg CM, et al. Dilatational band formation in bone. Proceedings of the National Academy of Sciences. 2012; 109:19178–19183.
20. Balooch G, Balooch M, Nalla RK, Schilling S, Filvaroff EH, Marshall GW, et al. TGF-beta regulates the mechanical properties and composition of bone matrix. Proc Natl Acad Sci USA. 2005; 102:18813–18818. [PubMed: 16354837]
21. Yang X, Matsuda K, Bialek P, Jacquot S, Masuoka HC, Schinke T, et al. ATF4 is a substrate of RSK2 and an essential regulator of osteoblast biology; implication for Coffin-Lowry Syndrome. Cell. 2004; 117:387–398. [PubMed: 15109498]
22. Jepsen KJ, Pennington DE, Lee YL, Warman M, Nadeau J. Bone brittleness varies with genetic background in A/J and C57BL/6J inbred mice. J Bone Miner Res. 2001; 16:1854–1862. [PubMed: 11585350]
23. Jepsen KJ, Akkus OJ, Majeska RJ, Nadeau JH. Hierarchical relationship between bone traits and mechanical properties in inbred mice. Mamm Genome. 2003; 14:97–104. [PubMed: 12584605]
24. Nyman JS, Makowski AJ, Patil CA, Masui TP, O'quinn EC, Bi X, et al. Measuring differences in compositional properties of bone tissue by confocal Raman spectroscopy. Calcif Tissue Int. 2011; 89:111–122. [PubMed: 21597909]
25. Turner CH, Burr DB. Basic biomechanical measurements of bone: a tutorial. Bone. 1993; 14:595–608. [PubMed: 8274302]
26. Ritchie RO, Koester KJ, Ionova S, Yao W, Lane NE, Ager JW III. Measurement of the toughness of bone: A tutorial with special reference to small animal studies. Bone. 2008; 43:798–812. [PubMed: 18647665]
27. Ritchie RO, Koester KJ, Ionova S, Yao W, Lane NE, Ager JW. Erratum: Measurement of the toughness of bone: a tutorial with special reference to small animal studies. Bone. 2008; 43:798–812. [PubMed: 18647665]
28. Takahashi Y. Evaluation of leak-before-break assessment methodology for pipes with a circumferential through-wall crack. Part I: stress intensity factor and limit load solutions. International Journal of Pressure Vessels and Piping. 2002; 79:385–392.
29. Lieber CA, Mahadevan-Jansen A. Automated method for subtraction of fluorescence from biological Raman spectra. Appl Spectrosc. 2003; 57:1363–1367. [PubMed: 14658149]
30. Maher JR, Takahata M, Awad HA, Berger AJ. Raman spectroscopy detects deterioration in biomechanical properties of bone in a glucocorticoid-treated mouse model of rheumatoid arthritis. J Bio med Opt. 2011; 16:087012.
31. Oliver WC, Pharr GM. Improved technique for determining hardness and elastic modulus using load and displacement sensing indentation experiments. J Mater Res. 1992

32. Kazanci M, Roschger P, Paschalis EP, Klaushofer K, Fratzl P. Bone osteonal tissues by Raman spectral mapping: orientation-composition. J Struct Biol. 2006; 156:489–496. [PubMed: 16931054]
33. Makowski AJ. Polarization control of Raman spectroscopy optimizes the assessment of bone tissue. J Biomed Opt. 2013; 18:055005.
34. Inzana JA, Maher JR, Takahata M, Schwarz EM, Berger AJ, Awad HA. Bone fragility beyond strength and mineral density: Raman spectroscopy predicts femoral fracture toughness in a murine model of rheumatoid arthritis. Journal of Biomechanics. 2013; 46:723–730. [PubMed: 23261243]
35. Ionova-Martin SS, Wade JM, Tang S, Shahnazari M, Ager JW, Lane NE, et al. Changes in cortical bone response to high-fat diet from adolescence to adulthood in mice. Osteoporos Int. 2011; 22:2283–2293. [PubMed: 20941479]
36. Ionova-Martin SS, Do SH, Barth HD, Szadkowska M, Porter AE, Ager JW, et al. Reduced size-independent mechanical properties of cortical bone in high-fat diet-induced obesity. Bone. 2010; 46:217–225. [PubMed: 19853069]
37. Davis MS, Kovacic BL, Marini JC, Shih AJ, Kozloff KM. Increased susceptibility to micro damage in Brtl/+ mouse model for osteogenesis imperfecta. Bone. 2012; 50:784–791. [PubMed: 22207275]
38. Burr DB. The contribution of the organic matrix to bone's material properties. Bone. 2002; 31:8–11. [PubMed: 12110405]
39. Currey JD. Effects of differences in mineralization on the mechanical properties of bone. Philos Trans R Soc Lond, B, Biol Sci. 1984; 304:509–518. [PubMed: 6142490]
40. Giraud-Guille MM. Twisted plywood architecture of collagen fibrils in human compact bone osteons. Calcif Tissue Int. 1988; 42:167–180. [PubMed: 3130165]
41. Reznikov N, Almany-Magal R, Shahar R, Weiner S. Three-dimensional imaging of collagen fibril organization in rat circumferential lamellar bone using a dual beam electron microscope reveals ordered and disordered sub-lamellar structures. Bone. 2013; 52:676–683. [PubMed: 23153959]
42. Schinke T, Karsenty G. Characterization of Osf1, an osteoblast-specific transcription factor binding to a critical cis-acting element in the mouse Osteocalcin promoters. J Biol Chem. 1999; 274:30182–30189. [PubMed: 10514508]
43. Xiao G, Jiang D, Ge C, Zhao Z, Lai Y, Boules H, et al. Cooperative interactions between activating transcription factor 4 and Runx2/Cbfa1 stimulate osteoblast-specific osteocalcin gene expression. J Biol Chem. 2005; 280:30689–30696. [PubMed: 16000305]
44. Yu S, Franceschi RT, Luo M, Zhang X, Jiang D, Lai Y, et al. Parathyroid hormone increases activating transcription factor 4 expression and activity in osteoblasts: requirement for osteocalcin gene expression. Endocrinology. 2008; 149:1960–1968. [PubMed: 18187540]
45. Fantner GE, Hassenkam T, Kindt JH, Weaver JC, Birkedal H, Pechenik L, et al. Sacrificial bonds and hidden length dissipate energy as mineralized fibrils separate during bone fracture. Nat Mater. 2005; 4:612–616. [PubMed: 16025123]
46. Zappone B, Thurner PJ, Adams J, Fantner GE, Hansma PK. Effect of Ca2+ ions on the adhesion and mechanical properties of adsorbed layers of human osteopontin. Biophysical Journal. 2008; 95:2939–2950. [PubMed: 18586839]
47. Ducy P, Desbois C, Boyce B, Pinero G, Story B, Dunstan C, et al. Increased bone formation in osteocalcin-deficient mice. Nature. 1996; 382:448–452. [PubMed: 8684484]
48. Boskey AL, Gadaleta S, Gundberg C, Doty SB, Ducy P, Karsenty G. Fourier transform infrared micro spectroscopic analysis of bones of osteocalcin-deficient mice provides insight into the function of osteocalcin. Bone. 1998; 23:187–196. [PubMed: 9737340]
49. Kavukcuoglu NB, Patterson-Buckendahl P, Mann AB. Effect of osteocalcin deficiency on the nanomechanics and chemistry of mouse bones. Journal of the Mechanical Behavior of Biomedical Materials. 2009; 2:348–354. [PubMed: 19627841]
50. Lian N, Lin T, Liu W, Wang W, Li L, Sun S, et al. Transforming Growth Factor β Suppresses Osteoblast Differentiation via the Vimentin Activating Transcription Factor 4 (ATF4) Axis. J Biol Chem. 2012; 287:35975–35984. [PubMed: 22952236]
51. Janssens K, Dijke ten P, Janssens S, Van Hul W. Transforming growth factor-beta1 to the bone. Endocr Rev. 2005; 26:743–774. [PubMed: 15901668]

52. Yu S, Franceschi RT, Luo M, Fan J, Jiang D, Cao H, et al. Critical role of activating transcription factor 4 in the anabolic actions of parathyroid hormone in bone. PLoS ONE. 2009; 4:e7583. [PubMed: 19851510]

53. Wang X, Guo B, Li Q, Peng J, Yang Z, Wang A, et al. miR-214 targets ATF4 to inhibit bone formation. Nat Med. 2013; 19:93–100. [PubMed: 23223004]

Highlights

- A transcription factor important to osteoblast differentiation influences bone toughness and fracture toughness but not material strength.
- Loss of ATF4 increases the amount of mineral relative to the amount of collagen.
- Regression analyses of polarization-sensitive vs. insensitive Raman peak ratios indicate tissue organization contributes to bone brittleness with ATF4 deficiency.

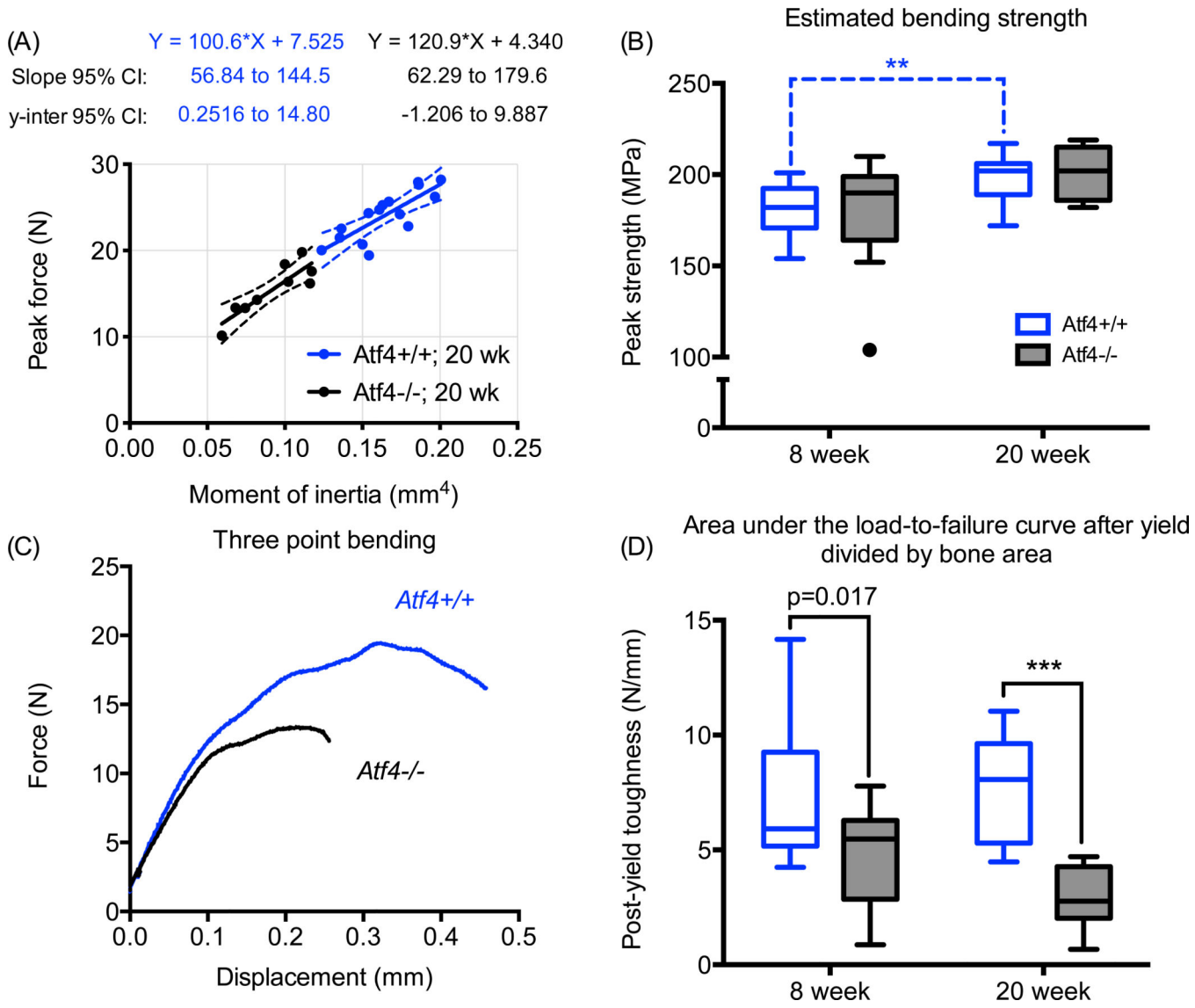

Figure 1.

Effect of ATF4 deletion on the biomechanical properties of cortical bone. Because they are narrower in cross-section, the femur mid-shafts from *Atf4*−/− mice were structurally weaker than those from wild-type mice (A). However, when accounting for structure, there was no difference in the estimated material strength between genotypes (B). Strikingly, ATF4-deficient bones sustained much less post-yield deformation (C) and thus were brittle (D). **p<0.005, ***p<0.0005; otherwise uncorrected p-value.

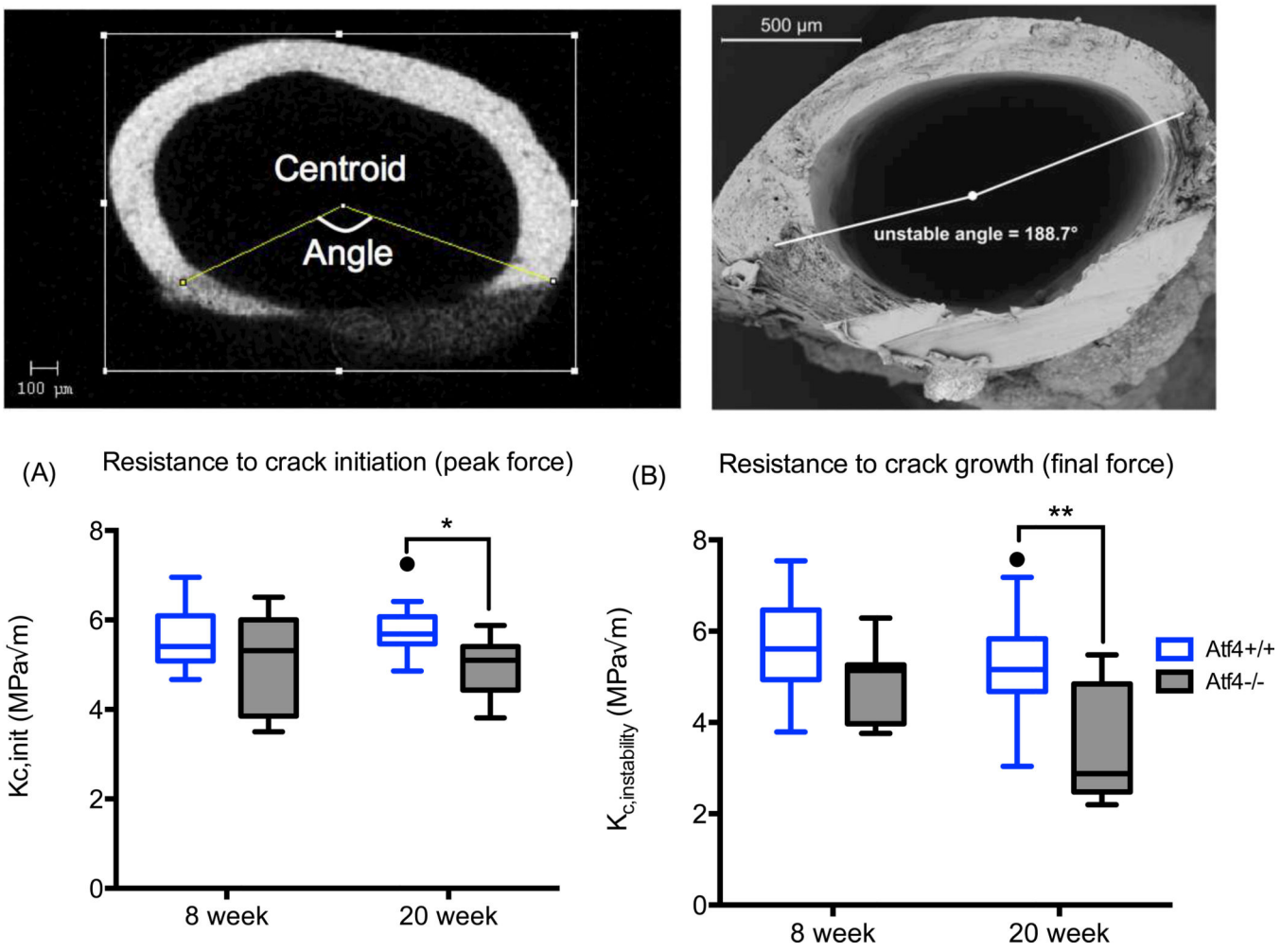

Figure 2.

Effect of ATF4 deletion on the fracture toughness of cortical bone. Whether determined for the initial notch angle using µCT (A) or for the angle at which crack propagation became instable (B) using SEM, the fracture toughness of bone was less for *Atf4*−/− than for *Atf4*+/+ mice by 20 weeks of age. *p<0.05, **p<0.005

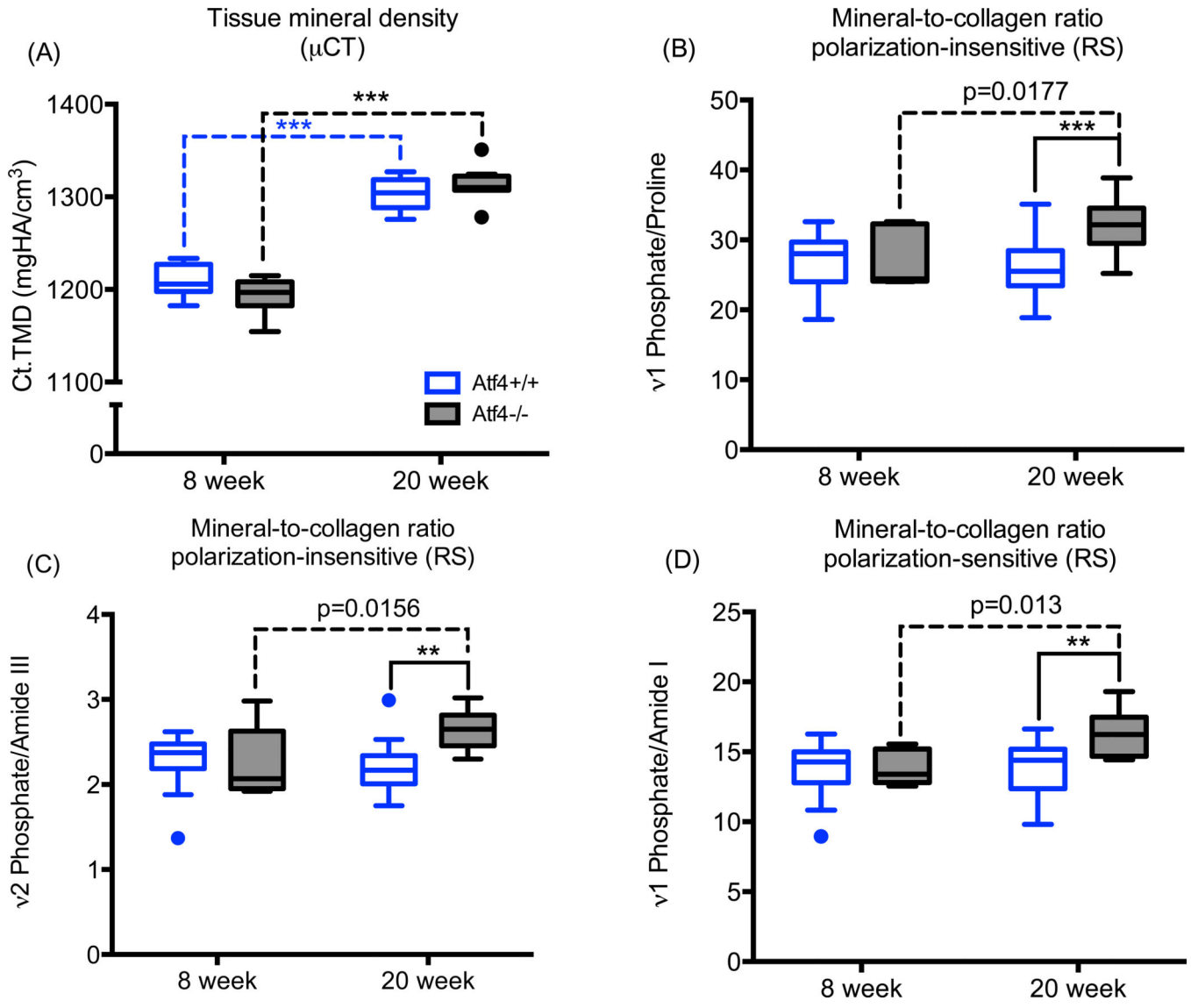

Figure 3.

Effect of ATF4 deletion on mineralization. As determined by μCT analysis of the notched femur (A), there was an age-related increase in tissue mineral density but no difference between genotypes. Regardless of whether the peak ratio from RS analysis of notched femur (anterior side) is not sensitive to polarization bias (B & C) or is sensitive (D), the mineral relative to collagen was greater in ATF4-deficient tissue at 20 weeks of age. *p<0.05, **p<0.005, ***p<0.0005; otherwise uncorrected p-value.

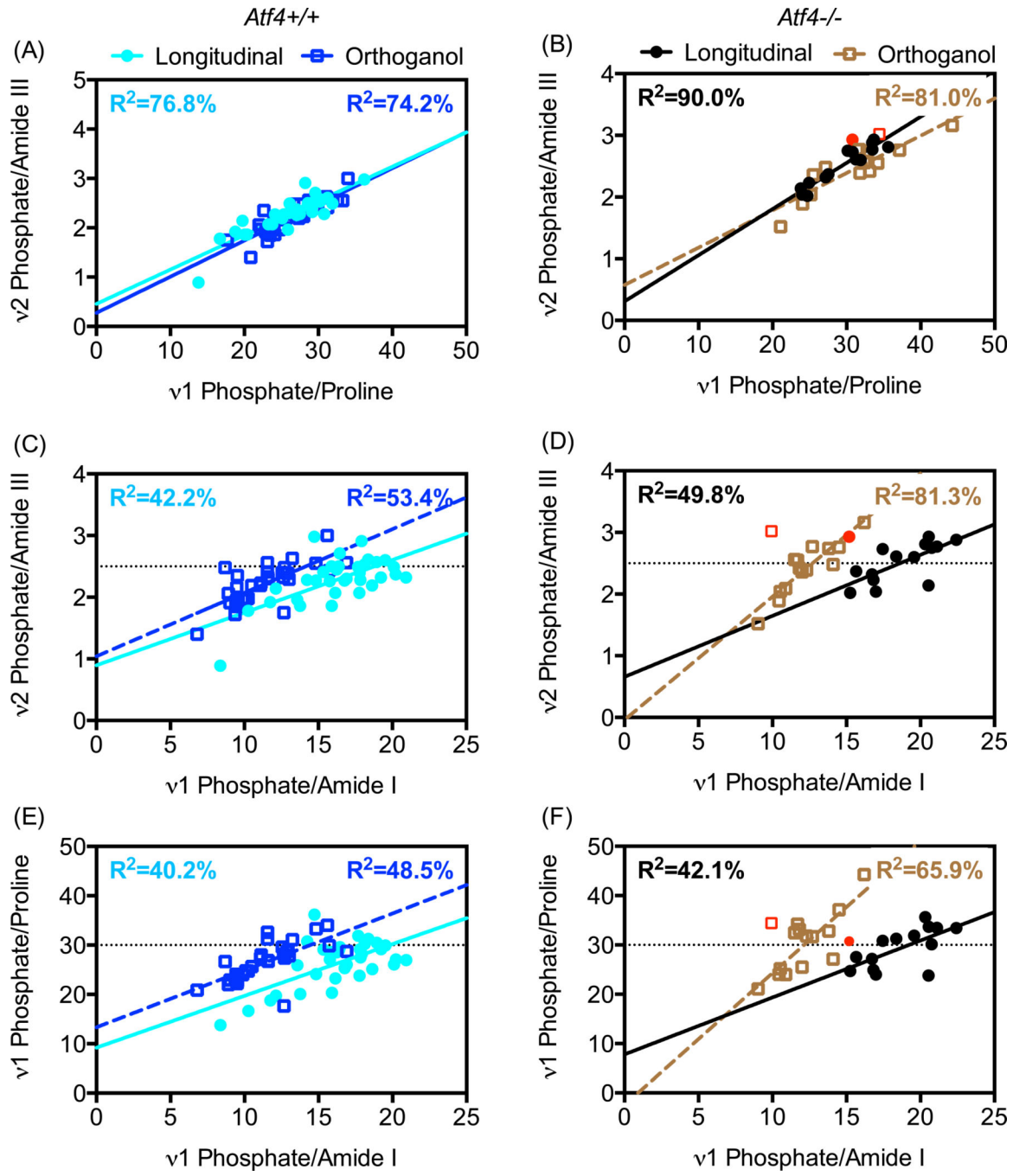

Figure 4.

Effects of bone orientation relative to light polarization on peak ratio relationships. Rotating the bone by 90° has little effect on the relationship between two different polarization-insensitive peak ratios (regression lines overlap in A and B). However, bone rotation does affect the relationships between a polarization-insensitive peak ratio and the polarization-sensitive peak ratios of MCR (C – D). The shift in the regression line for the Atf4+/+ bone (C & E) is less than the shift in regression line for Atf4−/− bone (D & F). Data from 8 wk and 20 wk mice were pooled. Data from 1 bone (red symbols) was removed from regression analyses because ν1Phos/AmI was an outlier in both orientations.

Table 1

Mean ± SD of selected properties of the L6 vertebra as determined by μCT analysis and compression testing (unadjusted p-values provided for *Atf4*+/+ vs. *Atf4*−/− within age group).

		8 wk			20 wk		
Property	**Unit**	**Atf4+/+**	**Atf4−/−**	**p-value**	**Atf4+/+**	**Atf4−/−**	**p-value**
BV/TV	−	0.247±0.032	0.147±0.030	<0.001	0.238±0.049	0.131±0.041	<0.001
Tb.N[a]	1/mm	5.32±0.43	4.58±0.42	0.001	4.95±0.59	3.80±0.40	<0.001
Tb.Th	mm	0.046±0.003	0.039±0.003	<0.001	0.048±0.003	0.041±0.005	<0.001
Tb.Sp[b]	mm	0.190±0.015	0.220±0.023	<0.001	0.205±0.029	0.267±0.028	<0.001
Conn.D[a]	1/mm^3	330.5±48.0	275.0±70.7	0.013[NS]	223.3±46.7	133.8±30.4	<0.001
Tb.TMD[a]	mgHA/cm^3	898±17	882±26	0.104[NS]	939±23	924±23	0.119[NS]
Peak force	N	32.6±6.4	15.3±4.2	<0.001	35.9±8.7	21.3±5.8	<0.001

[a] There were significant differences between age groups, irrespective of genotype;

[b] There was a significant difference between age groups within the knock-out mice;

[NS] Not-significant: To control for the family-wise error-rate, statistically significant differences occurred at p-values < 0.013 (Šidák correction).

Table 2

Mean ± SD or *median (25%, 75% quartile)* of selected properties of the femur mid-shaft as determined by calipers, μCT analysis and three point bending tests (unadjusted p-values provided for *Atf4*+/+ vs. *Atf4*−/− within age group).

		8 wk			20 wk		
Property	**Unit**	**Atf4+/+**	**Atf4−/−**	**p-value**	**Atf4+/+**	**Atf4−/−**	**p-value**
Length	mm	13.7±0.5	12.2±0.8	<0.001	14.5 ±0.6	12.9 ±0.5	<0.001
Tt.Ar[b]	mm^2	*1.84 (1.74, 1.95)*	*1.31 (1.26, 1.71)*	0.027*NS*	*1.99 (1.92, 2.13)*	*1.55 (1.40, 1.68)*	*<0.001*
Ct.Ar[b]	mm^2	0.797±0.078	0.680±0.194	0.013*NS*	0.928±0.073	0.707±0.077	<0.001
Imin[b]	mm^4	0.135±0.023	0.097±0.056	0.007	0.165±0.023	0.092±0.022	<0.001
Ma.V	mm^3	1.17±0.15	0.96±0.29	0.011	1.20±0.10	0.93±0.21	0.001
Ct.Th[b]	mm	0.180±0.015	0.169±0.020	0.119*NS*	0.206±0.014	0.180±0.019	0.001
Ct.TMD[a]	$mgHA/cm^3$	1147±33	1173±25	0.025*NS*	1263±22	1290±22	0.020*NS*
Stiffness[a]	N/mm	104±23	72±26	<0.001	139±19	98±17	<0.001
Peak force[b]	N	18.5±3.5	13.0±3.5	<0.001	24.1±2.9	15.5±3.0	<0.001
PYD	mm	0.317±0.152	0.259±0.145	0.258*NS*	0.341±0.111	0.161±0.087	0.001

[a] There were significant differences between age groups, irrespective of genotype;

[b] There was a significant difference between age groups within the wild-type mice;

NS Not-significant: To control for the family-wise error-rate, statistically significant differences occurred at p-values < 0.013 (Šidák correction).

Table 3

Mean ± SD or *median (25%, 75% quartile)*of selected tissue properties acquired from the tibia cross-section as determined by Raman spectroscopy and nanoindentation (unadjusted p-values provided for Atf4+/+ vs. Atf4−/− within age group).

		8 wk			20 wk		
Property	**Unit**	**Atf4+/+**	**Atf4−/−**	**p-value**	**Atf4+/+**	**Atf4−/−**	**p-value**
Modulus[a]	GPa	27.2±2.3	25.1±3.7	0.029[NS]	30.7±1.7	29.6±2.1	0.337[NS]
Hardness[a]	*GPa*	*1.03 (0.96, 1.10)*	*0.94 (0.83, 1.06)*	0.173[NS]	*1.12 (1.03, 1.17)*	*1.13 (1.08, 1.20)*	0.429[NS]
ν1Phos/AmI[c]	–	11.2±1.0	10.4±0.7	0.006	11.6±0.7	12.3±0.6	0.025[NS]
ν2Phos/AmIII[c]	–	*1.88 (1.84, 1.91)*	*1.85 (1.66, 1.90)*	0.262[NS]	*1.90 (1.85, 1.98)*	*1.99 (1.98, 2.05)*	0.009
Carb/ν1Phos[b]	–	*0.154 (0.151, 0.161)*	*0.166 (0.157, 0.185)*	0.007	*0.175 (0.167, 0.179)*	*0.178 (0.176, 0.179)*	0.270[NS]
$[FWHM]^{-1}$	–	*0.0630 (0.0620, 0.0632)*	*0.0628 (0.0567, 0.0692)*	0.010	*0.0630 (0.0627, 0.0631)*	*0.0627 (0.0625, 0.0627)*	0.123[NS]

[a]There were significant differences between age groups, irrespective of genotype;

[b]There was a significant difference between age groups within the wild-type mice;

[c]There was a significant difference between age groups within the knock-out mice;

[NS]Not-significant: To control for the family-wise error-rate, statistically significant differences occurred at p-values < 0.013 (Šidák correction)

Table 4

General linear equations of the best-fit models to 3 different peak ratio combinations of the mineral to collagen ratio for each genotype in which orientation of the bone relative to polarization axis changed by 90 °(L – longitudinal and O – orthogonal).

Atf4+/+			*Atf4*−/−		
Best-fit Regression Model	**Orientation p-value**	**R^2**	**Best-fit Regression Model**	**Orientation p-value**	**R^2**
ν2Phos/AmIII = 0.42 + 0.071 × ν1Phos/Prol if L or O	0.105	75.9	ν2Phos/AmIII = 0.62 + 0.065 × ν1Phos/Prol if L ν2Phos/AmIII = 0.46 + 0.065 × ν1Phos/Prol if O	0.005	80.7
ν1Phos/Proline = 12.52 + 0.85 × ν1Phos/AmI if L ν1Phos/Proline = 16.82 + 0.85 × ν1Phos/AmI if O	0.006	43.3	ν1Phos/Proline = 16.78 + 0.68 × ν1Phos/AmI if L ν1Phos/Proline = 2.64 + 2.26 × ν1Phos/AmI if O	0.038[a]	58.5
ν2Phos/AmIII= 0.92 + 0.084 × ν1Phos/AmI if L ν2Phos/AmIII= 1.26 + 0.084 × ν1Phos/AmI if O	0.014	47.2	ν2Phos/AmIII= 1.08 + 0.076 × ν1Phos/AmI if O ν2Phos/AmIII= 0.36 + 0.17 × ν1Phos/AmI if L	0.059[a]	70.1

[a] p-value for the interaction between orientation and peak ratio.